Frontiers in Bioscience Landmark

Front. Biosci. (Landmark Ed) **2026**; 31(6): 49794
https://doi.org/10.31083/FBL49794

Original Research

SPI1 Promotes Intracranial Aneurysm Formation by Inhibiting Wnt5a Transcription

ZengShi Li[1,2], WeiChen Wang[2], Wei Li[2], Jie Peng[2], JunXi Liu[1], Yi Wu[1,3,*]

[1]School of Medicine, Hunan Normal University, 410000 Changsha, Hunan, China
[2]Department of Neurosurgery, Changsha First Hospital, 410000 Changsha, Hunan, China
[3]Department of Laboratory Medicine, Hunan Provincial People's Hospital (The First Affiliated Hospital of Hunan Normal University), 410005 Changsha, Hunan, China
*Correspondence: yizhonglzs@163.com; Wuyi19701210@sina.com (Yi Wu)

Academic Editors: Amelia Casamassimi and Thomas Heinbockel
Submitted: 7 January 2026 Revised: 16 April 2026 Accepted: 9 May 2026 Published: 24 June 2026

Abstract

Background: SPI1 is a hub gene associated with intracranial aneurysms (IA) and is highly expressed in IA tissues. However, its functional role in IA formation remains unclear. This study aimed to investigate the effect of SPI1 on IA development and its underlying mechanisms. **Methods**: An *in vitro* IA cell model was established using Platelet-Derived Growth Factor BB (PDGF-BB)-induced vascular smooth muscle cells (VSMCs). SPI1 expression was silenced via sh-SPI1 plasmids to assess its effects on VSMC phenotypic switching and the Wnt pathway. The binding of SPI1 to the Wnt5a promoter was verified by chromatin immunoprecipitation (ChIP) assays. Furthermore, to investigate whether SPI1 influences the contractile-to-synthetic phenotypic transition of VSMCs via the Wnt pathway, the cells were treated with the Wnt5a inhibitor Box5. The *in vivo* effects of SPI1 knockdown were assessed using an IA mouse model. **Results**: Compared with the control group, PDGF-BB treatment increased the expression of SPI1, synthetic phenotype markers (MMP3/9), and Wnt pathway-related proteins (β-catenin and c-Myc), while reducing the expression of contractile markers (α-SMA and SM22α) and Wnt5a. Silencing of SPI1 reversed these changes. ChIP assays further confirmed that SPI1 could bind directly to the Wnt5a promoter. Moreover, treatment with the Wnt5a inhibitor Box5 reversed the SPI1 knockdown-induced changes in Wnt5a, β-catenin, and c-Myc in VSMCs. *In vivo*, SPI1 knockdown alleviated vascular wall thickening in the cerebral artery ring of IA mice, improved the loss of elastic fibers, and suppressed inflammatory responses. In addition, SPI1 knockdown promoted Wnt5a expression while restoring the expression of β-catenin, c-Myc, and phenotypic markers toward control levels. **Conclusion**: This study suggests that SPI1 promotes intracranial aneurysm formation by inhibiting Wnt5a transcription, thereby promoting activation of the canonical Wnt/β-catenin pathway and driving VSMC phenotypic switching toward a synthetic phenotype. *In vivo*, SPI1 knockdown alleviated vascular wall injury and inflammation. These findings indicate that the SPI1/Wnt5a signaling axis may represent a potential therapeutic target for intracranial aneurysms.

Keywords: intracranial aneurysm; SPI1; Wnt5a; vascular smooth muscle cells; phenotypic switching

1. Introduction

Intracranial aneurysm (IA) is a cerebrovascular disease characterized by localized abnormal enlargement of the lumen of a cerebral artery, commonly seen in middle-aged and elderly patients [1,2], with an incidence rate of approximately 3% [3,4]. These aneurysms are prone to sudden rupture during episodes of stress, physical exertion, fatigue, or other conditions associated with elevated blood pressure. Once ruptured, they can cause acute subarachnoid hemorrhage, which is associated with high rates of disability and mortality [4,5,6]. Currently, the main treatment strategies for IA include endovascular coil embolization and surgical clipping [7,8]. However, these interventions may also cause a range of complications and have a relatively high recurrence rate. Therefore, elucidating the pathogenesis of IA and the underlying molecular mechanisms is of substantial importance for identifying diagnostic markers and developing drugs to prevent the progression of IA [9,10].

The pathogenesis of IA is complex, and its development may be related to various factors, including atherosclerosis, hypertension, and smoking [11]. These factors contribute to endothelial injury, vascular wall degeneration, vascular smooth muscle cell phenotypic modulation, inflammation, and cell death, leading to vascular cell loss and extracellular matrix degradation [12,13]. Among these mechanisms, vascular smooth muscle cells (VSMCs) are the predominant cellular component of the arterial wall and are essential for maintaining vascular wall integrity and mechanical properties through the production of extracellular matrix. Their structural and pathological alterations play a fundamental role in the progression and rupture of IA [14,15,16]. Under physiological conditions, VSMCs mainly exhibit a contractile phenotype, which is characterized by high expression of contractile markers such as α-SMA and SM22α. However, when vessels are exposed to pathological stimuli, VSMCs undergo phenotypic switching toward a synthetic state, accompanied by

increased expression of the synthetic marker osteopontin (OPN) [17,18], which leads to the significant enhancement of cellular secretion, proliferation, and migration capabilities [17]. Furthermore, the expression of matrix metalloproteinases (MMPs) is also significantly increased. This phenotypic switching of VSMCs ultimately accelerates the formation and rupture of IA [15,18]. Therefore, investigating the molecular mechanisms that regulate VSMC phenotypic switching may provide new insights and therapeutic strategies for IA.

The SPI1 gene encodes PU.1, a transcription factor from the E26 transformation-specific (ETS) family [19]. PU.1 plays a central role in regulating immune cell differentiation and functional activity and has been implicated in the pathophysiology of autoimmune disorders [20]. SPI1 is located on chromosome 11p11.22 and functions as a key transcriptional regulator [21]. In recent years, accumulating evidence has demonstrated that SPI1 is involved in the progression of multiple malignancies, including cervical, gastric, and liver cancers [22,23,24]. For example, SPI1 promotes the migration and invasion of gastric cancer cells by upregulating NMT1 through activation of the PI3K/AKT/mTOR signaling pathway [25], while in hepatocellular carcinoma, SPI1 is recruited by LINC00324 to promote the expression of Fas ligand, thereby facilitating tumor progression [26]. Traditionally, SPI1 has been recognized for its role in regulating the differentiation of hematopoietic stem cells into myeloid and lymphoid cells. However, recent studies have extended its functional scope, revealing that SPI1 also possesses direct pathophysiological effects in vascular cells [27]. Notably, SPI1 has been identified as a key immunomodulatory factor in acute myocardial infarction, where its upregulation is closely associated with increased proinflammatory immune cell infiltration and reduced protective immune cells. Mechanistically, SPI1 directly activates the TLR4/NF-κB signaling axis, thereby promoting cardiomyocyte apoptosis, inflammatory responses, and tissue fibrosis, highlighting its potential as both a diagnostic biomarker and a therapeutic target through modulation of immune-inflammatory pathways [28,29]. In addition, SPI1 has been reported to be upregulated in cardiomyocytes and to play a regulatory role in the progression of atherosclerosis [30], which is a recognized risk factor for IA. Furthermore, analysis of Gene Expression Omnibus (GEO) datasets has identified SPI1 as a hub gene associated with IA, with significantly elevated expression observed in IA tissues [31]. Based on these findings, we hypothesize that SPI1 may act as a pathogenic regulator in IA; however, further experimental validation is required to substantiate this hypothesis.

The Wnt protein family is a class of secreted glycoproteins rich in cysteine residues [32]. Wnt signaling pathways are mainly divided into canonical β-catenin-dependent pathways and non-canonical β-catenin-independent pathways [33]. The non-canonical pathways primarily comprise the Wnt/planar cell polarity (PCP) pathway and the Wnt/Ca^{2+} pathway. The Wnt/PCP pathway regulates cytoskeletal organization to control cell polarity and migration, whereas the Wnt/Ca^{2+} pathway modulates intracellular Ca^{2+} signaling to influence cell fate determination and motility through downstream transcriptional responses [34]. The Wnt signaling network plays a critical regulatory role in a wide range of pathological conditions, including cardiovascular diseases, cancer, metabolic disorders, and autoimmune diseases [35]. Wnt5a is a representative Wnt ligand that predominantly activates β-catenin-independent signaling pathways. In addition to its role in regulating cellular development and differentiation, Wnt5a is closely associated with various pathological processes, including cardiovascular disease, tumor progression, metabolic abnormalities, tissue fibrosis, and developmental disorders [35,36,37]. It is worth noting that Wnt5a signaling is highly context-dependent, with its functional effects varying according to receptor composition [38,39], cellular microenvironment [40,41], and specific pathological conditions [42,43]. For example, independent of Bruton's tyrosine kinase (BTK), Wnt5a can activate ERK1/2 through a ROR1/DOCK2-dependent pathway, thereby promoting the proliferation of chronic lymphocytic leukemia cells [44]. In vascular pathology, the Wnt5a/Ror2 axis has been shown to promote atherosclerosis by inhibiting ABCA1 and activating NF-κB signaling, leading to cholesterol accumulation and inflammation in VSMCs [35]. Moreover, activation of the non-canonical Wnt5a–PCP pathway by CTHRC1 regulates cardiac fibroblast-mediated scar formation, which is essential for maintaining myocardial structural integrity after infarction [45]. Our previous work further demonstrated that miR-374a-5p targets Wnt5a to regulate VSMC phenotypic switching and M2 macrophage polarization, thereby contributing to IA progression [46]. However, the potential connection between SPI1 and Wnt5a, and its relevance to IA pathogenesis, remains to be elucidated.

In this present study, we aimed to characterize the expression pattern and functional role of SPI1 in IA models and determine whether SPI1 regulates IA formation and progression through Wnt5a-mediated Wnt signaling. To our knowledge, these findings provide a basis for identifying potential therapeutic targets and offer mechanistic insights for future studies on IA prevention and treatment.

2. Materials and Methods

2.1 Cell Culture

Human cerebral vascular smooth muscle cells (VSMCs) (CP-H116, Procell, China) were cultured in Ham's F-12K medium (21127022, Gibco, USA) supplemented with 10% fetal bovine serum (FBS) (A5670701, Gibco, USA) and 1% dual antibiotics (15140148, Gibco, USA) at 37°C in a humidified incubator with 5% CO_2, and cells within passage 3 were used for all experiments. [47]. All experiments in this study were performed using cells derived from three independent donors (biological

triplicates) to ensure the generalizability of the results. All cell lines were validated by STR profiling and tested negative for mycoplasma contamination.

2.2 Cell Treatment

The cells were divided into four groups: Control, Platelet-Derived Growth Factor BB (PDGF-BB), sh-NC, and sh-SPI1. PDGF-BB (10 ng/mL, HY-P7055B, MCE, USA) [14,46] was added to serum-free Ham's F-12K medium, and the cells were incubated for 24 hours at 37 °C to induce phenotypic switching. VSMCs in the sh-SPI1 and sh-NC groups were transfected for 24 hours with silencing transfection reagent (sh-SPI1) or negative control transfection reagent (sh-NC), respectively, using Lipofectamine 2000 (11668019, Invitrogen, USA). After transfection, VSMCs were treated with or without the Wnt5a inhibitor Box5 (100 μM, HY-123071, MCE, USA) for 2 hours [46,48], with DMSO serving as the control. The SPI1 shRNA sequence was 5′-GCCCTATGACACGGATCTATA-3′, and the NC shRNA sequence was 5′-GAGGAAAGGATTGAGTTTAGC-3′.

2.3 Animal Treatment

Male C57 mice (6–8 weeks old, 20-25 g) were purchased from Changsha Tianqin Biotechnology Co., Ltd. All mice were provided with food and water ad libitum and acclimated for one week. Inclusion criteria: healthy mice with normal activity and no signs of infection or illness were included. Exclusion criteria: mice that died during or within 48 hours after surgery, or showed signs of severe infection or surgical failure, were excluded. The animals were then randomly divided into four groups: Control, IA, sh-NC, and sh-SPI1, with six mice in each group. No animals were excluded from the study. After acclimation, all mice except those in the Control group underwent ligation of the left common carotid artery and the posterior branches of the bilateral renal arteries. One week after surgery, the mice were anesthetized with 1% isoflurane inhalation, the scalp was shaved and disinfected, and the animals were fixed in a stereotaxic instrument. A 1 cm midline incision was made, the subcutaneous fascia was dissected, and the skull was fully exposed. The coordinates for *in situ* injection were set at 1.0 mm to the right of the anterior fontanelle (X-axis), 2.5 mm posterior to the anterior fontanelle, and 5.3 mm in depth. Elastase (1 μL, E1250, Sigma, GER) was injected at a rate of 0.2 μL/min [49]. Concurrently, mice were provided with 1% NaCl drinking water. After model establishment, mice in the sh-NC and sh-SPI1 groups received tail vein injections of 2×10^{11} vg adeno-associated virus (AAV)-shNC or AAV-shSPI1, respectively. Angiotensin II (A1042, APExBIO, USA) was subsequently administered via intraperitoneal injection. The AAV serotype used in this study was AAV9, which was constructed and packaged by HonorGene Company. After recovery, mice were fed a diet containing 0.12% BAPN and 8% NaCl for four weeks. At the experimental endpoint, all mice were humanely euthanized in accordance with established protocols [50]. Briefly, mice were anesthetized with 5% isoflurane inhalation and euthanized by cervical dislocation [51]. All animal experiments were conducted in accordance with ARRIVE guidelines and approved by the Ethics Committee of Changsha First Hospital.

2.4 Evaluation of Aneurysm Formation and Rupture

To assess aneurysm rupture, two researchers not involved in the experimental grouping performed daily neurological function assessments in the mice according to previously reported methods [52]. The scoring criteria were as follows: 0 points (normal); 1 point (weight loss >2 g within 24 hours); 2 points (flexion of the trunk and forelimbs when the tail is lifted); 3 points (rotation at rest with normal posture); 4 points (tilting to one side at rest); and 5 points (no spontaneous activity). Mice exhibiting neurological symptoms (score ≥1) were immediately euthanized, and the circle of Willis was examined under a microscope post-mortem to confirm the presence of aneurysms and subarachnoid hemorrhage. Asymptomatic mice were euthanized after 4 weeks, and the circle of Willis was harvested for HE and Victoria blue staining to assess the formation of aneurysms.

2.5 Reverse Transcription Quantitative Polymerase Chain Reaction (RT-qPCR)

Total RNA was extracted from cells or tissues using TRIzol reagent (15596026, Thermo, USA). cDNA was synthesized using an mRNA reverse transcription kit (CW2569, Cwbio, China) with mRNA as the template. The resulting cDNA was mixed with the fluorescent dye UltraSYBR mixture (CW2601, Cwbio, China) and subjected to RT-qPCR with real-time fluorescence signal detection. GAPDH was used as the internal reference gene, and the relative expression levels of target genes were calculated using the $2^{-\Delta\Delta CT}$ method. The primer sequences are listed in Table 1.

2.6 Western Blot (WB)

RIPA lysis buffer (AWB0136, Abiowell, China) was used to extract total protein from brain tissue and VSMCs. Proteins were transferred to nitrocellulose membranes after separation by electrophoresis. After blocking the membranes with 5% non-fat milk powder (AWB0004, Abiowell, China) for 90 minutes at room temperature, primary antibodies were added, diluted according to the ratios shown in Table 2, and incubated overnight at 4 °C. HRP-labeled secondary antibodies were diluted with PBST (AWI0130, Abiowell, China) (Table 2), and then incubated with the membrane at room temperature for 90 minutes. The membrane was incubated with ECL chemiluminescent solution (AWB0005, Abiowell, China) for 1 minute and then imaged using an imaging system (ChemiScope6100, Clinx, China). GAPDH was used as the internal reference. Im-

Table 1. Primer sequences used in this study.

Primers	Sequence	Product length /bp
H-GAPDH	F ACAGCCTCAAGATCATCAGC R GGTCATGAGTCCTTCCACGAT	104
H-SPI1	F ATCCTGAGGGGCTCTGCATTG R ACGAGGGGAAACCCTTCCAT	104
H-MMP3	F TGAGGACACCAGCATGAACC R ACTTCGGGATGCCAGGAAAG	248
H-MMP9	F CTGAAGGCCATGCGAACCCCA R GCAAAGGCGTCGTCAATCACC	155
H-α-SMA	F CTATGAGGGCTATGCCTTGCC R GCTCAGCAGTAGTAACGAAGGA	122
H-SM22α	F CCTCTGACACATGCGGCTT R AGTCATTCCAGGTCGGCATC	114
H-Wnt5a	F AATTCTGGCTCCACTTGTTGCT R ACATTGCACTTCCAGCCATC	88
M-GAPDH	F GCGACTTCAACAGCAACTCCC R CACCCTGTTGCTGTAGCCGTA	122
M-SPI1	F GTGGCAGGCCCTTCGATAAA R CTACAGGAGCCCTGGGTGAG	81
M-MMP3	F TTCTGGGCTATACGAGGGCA R CTTCTTCACGGTTGCAGGGA	84
M-MMP9	F GCCCTGGAACTCACACGACA R GTAGCCCACGTCGTCCACC	139
M-α-SMA	F GCCCCTGAAGAGCATCCGAC R CCAGAGTCCAGCACAATACCAGT	179
M-SM22α	F CAGACACCGAAGCTACTCTCCT R GACTGCACTTCTCGGCTCA	106
M-Wnt5a	F ACTTGTTGCTCCGGCCCAG R GCGAAGGAGAAAAACGTGGC	123
Wnt5a#1	F TTTTAGTGTAGGCATTTAGC R ATTCCAGGTGGTTCAGTC	129
Wnt5a#2	F GGGGAATACTGGCTGACC R AGAGCCTGAAGAGGTAGAT	281
Wnt5a#3	F GGCAACGTGGGATCAGTG R TGTAGACAGCAAGCCATA	109

ageJ software (version 1.52v, National Institutes of Health, USA) was used to analyze the relative gray values of the target bands.

2.7 Cell Counting Kit-8 (CCK-8) Assay

VSMCs were seeded into 12-well plates at a density of 1×10^4 cells per well. After treatment, the drug-containing medium was removed, and 300 µL of CCK-8 working solution (NU679, Dojindo, Japan) was added to each well, followed by incubation at 37 °C for 4 hours. The supernatant was then transferred to a 96-well plate (3 replicates per group, 0030730119, Eppendorf, GER), and the absorbance was measured at 450 nm.

2.8 Transwell Migration Experiment

VSMCs were resuspended in serum-free medium and added to the upper chamber of the Transwell insert (3422, Corning, USA). Then, 500 µL of complete medium containing 10% FBS was added to the lower chamber. After incubation at 37 °C for 72 hours, the cells in the upper chamber were removed, and the migrated cells were fixed and stained with crystal violet (AWC0333, Abiowell, China). Three random fields were selected under the microscope for photography and counting.

2.9 TOP/FOP Flash Assay

293T cells (AW-CNH086, iCell, China) were maintained in DMEM supplemented with 10% FBS and 1% dual antibiotics at 37 °C in a humidified incubator with 5% CO_2. Cells within passage 5 were used for all experiments. Then, the cells were seeded into 24-well plates and co-transfected with TOP-Flash (WT) or FOP-Flash (MUT) reporter plasmids and sh-NC or sh-SPI1 (HonorGene, China). Plasmids were extracted using an endotoxin-free plasmid kit (DP117, TIANGEN, China). After 48 hours of transfection, the medium was discarded, and the cells were washed

Table 2. Antibody details of this study.

Name	Item number	Dilution ratio	Company
SPI1	55100-1-AP	1:1000	Proteintech (USA)
MMP3	AWA58491	1:1000	Abiowell (China)
MMP9	AWA12616	1:5000	Abiowell
SM22α	10493-1-AP	1:20,000	Proteintech
Wnt5a	55184-1-AP	1:2000	Proteintech
α-SMA	14395-1-AP	1:5000	Proteintech
β-Catenin	ab32572	1:5000	Abcam (UK)
C-myc	ab32072	1:1000	Abcam
GAPDH	10494-1-AP	1:5000	Proteintech
PCNA	10205-1-AP	1:5000	Proteintech
HRP goat anti-mouse IgG	SA00001-1	1:5000	Proteintech
HRP goat anti-rabbit IgG	SA00001-2	1:6000	Proteintech

with PBS. Subsequently, 100 µL of PLB lysis buffer was added to each well, and the cells were lysed at room temperature for 15 minutes. Then, 20 µL of cell lysate was mixed with 100 µL of LAR II reagent to measure firefly luciferase activity using the Dual-Luciferase Reporter Assay System (E1910, Promega, USA). The ratio of firefly to Renilla luciferase activity was calculated, and the relative luciferase activity was normalized to the sh-NC+WT control group.

2.10 Chromatin Immunoprecipitation (ChIP) and RT-qPCR

The cells were collected by trypsin digestion (15090046, Gibco, USA) and fixed with 1.1% formaldehyde (F8775, Sigma, GER) for 10 minutes. The reaction was then terminated with glycine (V900144, Sigma, GER). After centrifugation and washing, the cells were resuspended in Buffer B/C and centrifuged again to obtain the precipitate. Buffer D and proteinase inhibitors (AWH0645, Abiowell, China) were added to the pellet, followed by sonication (4 s on/6 s off, total 60 s, 20% power). The supernatant was then collected by centrifugation. The supernatant was mixed with ddH_2O and DNA purification slurry, denatured at 98 °C, and incubated at room temperature. Proteinase K (P1120, Solarbio, China) was used for stepwise digestion (55 °C/98 °C), and DNA fragments were analyzed by 1.5% agarose gel electrophoresis (111860, Biowest, ES). After sonication and dilution with 1× ChIP Buffer, the supernatant was divided into three groups: input, target antibody, and positive/negative control. The antibody was then incubated overnight at 4 °C. After cleaning, the agarose beads were combined with the sample and immunoprecipitated three times with ChIP Buffer. The agarose beads were resuspended in DNA purification slurry, evenly mixed with chromatin from the input group, denatured at 98 °C, and then incubated. After proteinase K digestion, 70 µL of supernatant was collected. Finally, the relative expression levels of the target gene were determined using RT-qPCR, as described in Section 2.5. The control IgG used in the experiment was normal rabbit IgG (30000-0-AP, Proteintech, USA), which matched the rabbit-derived SPI1 antibody (Ab302623, Abcam, China) used in this study. The primer sequences are shown in Table 1.

2.11 Hematoxylin-Eosin (HE) Staining

After baking at 60 °C for 2–3 hours, the tissue sections were dewaxed by immersion in xylene (10023418, SCRC, China) three times for 20 minutes each. They were then successively immersed in 100%, 95%, 85%, and 75% ethanol (W990001-1, Tianjin Zhiyuan, China) for 5 minutes each, followed by washing with distilled water for 5 minutes. The staining procedures were as follows: eosin (AWI0029a, Abiowell, China) staining for 1–5 minutes, followed by rinsing with distilled water and bluing; hematoxylin (AWI0001a, Abiowell, China) staining for 1–10 minutes. The sections were then dehydrated with 95% and 100% ethanol for 5 minutes each and cleared with xylene twice for 10 minutes each. Finally, the sections were mounted with neutral resin (AWI0238a, Abiowell, China), observed under a microscope (BA210T, Motic, China), and photographed.

2.12 Victoria Blue Staining

After baking at 60 °C for 12 hours, tissue sections were dewaxed three times in xylene, 20 minutes each. They were then successively immersed in 100%, 95%, 85%, and 75% ethanol for 5 minutes each, followed by washing with distilled water for 5 minutes. The sections were oxidized in Tanake oxidant for 5 minutes and washed with tap water, then bleached in Tanake bleaching agent for 2 minutes until the oxidant was completely decolorized. The sections were then washed twice with 70% ethanol for 10 seconds each until no staining solution remained, followed by rinsing with purified water. After staining with Victoria Blue (G1596, Solarbio, China) for 24 hours, the sections were rinsed twice with 70% ethanol for 10 seconds each. The nuclei were counterstained with nuclear red staining solution for 5–10 minutes and slightly washed with running water.

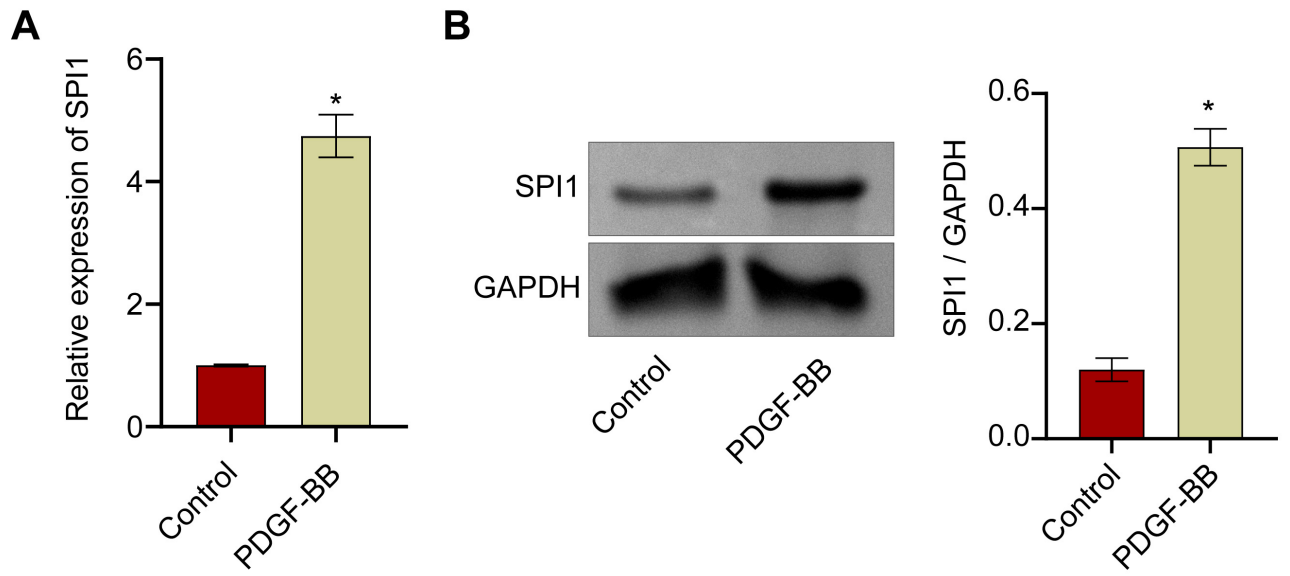

Fig. 1. SPI1 is markedly overexpressed in VSMCs induced by Platelet-Derived Growth Factor BB (PDGF-BB). (A) SPI1 expression in VSMCs was examined using RT-qPCR. (B) SPI1 expression in VSMCs was examined using WB. n = 3, *$p < 0.05$ vs. Control. VSMCs, vascular smooth muscle cells; RT-qPCR, reverse transcription quantitative polymerase chain reaction; WB, Western blot.

The sections were dehydrated with 95% and 100% ethanol for 5 minutes each and then cleared in xylene twice for 10 minutes each. Finally, the sections were sealed with neutral resin, observed under a microscope, and photographed.

2.13 Enzyme-linked Immunosorbent Assay (ELISA)

Fifty milligrams of fresh tissue were homogenized with precooled PBS on ice, centrifuged at 5000 × g at 2–8 °C for 5 minutes, and the supernatant was collected. Inflammatory factor levels were measured using commercial ELISA kits: TNF-α (KE10002, Proteintech, USA), IL-1β (KE10003, Proteintech, USA), IL-6 (KE10007, Proteintech, USA), and IL-10 (KE10103, Proteintech, USA). All steps were performed according to the manufacturer's instructions, and the optical density (OD) of each well was measured at 450 nm using an enzyme-linked immunosorbent assay reader (MB-530, HEALES, China).

2.14 Immunohistochemistry (IHC)

The expression of SPI1 in the circle of Willis of mice was detected by IHC. After dewaxing, antigen retrieval, and endogenous peroxidase blocking of tissue sections, mouse-derived SPI1 primary antibody (66618-2-Ig, Proteintech, USA) was added and incubated at 4 °C overnight. The secondary antibody (AWI0629, Abiowell, China) was then incubated at 37 °C for 30 minutes. DAB (34065, ThermoFisher, USA) was used for color development, hematoxylin (H8070, Solarbio, China) was used for counterstaining, and the sections were dehydrated, cleared, and sealed. Images were collected using an optical microscope (BA210T, Motic, China).

2.15 Statistical Analysis

Data are expressed as mean ± standard deviation (mean ± SD). The number of samples (n) represents the number of independent biological replicates. Statistical analyses were performed using GraphPad Prism 8. Student's *t*-test was used for comparisons between two groups, and one-way ANOVA followed by Tukey's multiple comparison test was used for comparisons among three or more groups. A p-value < 0.05 was considered statistically significant. Investigators performing histological evaluations (HE staining, Victoria blue staining, IHC) and ELISA assays were blinded to group allocation until all data were collected and analyzed. Statistical power was evaluated using the degrees of freedom (E), calculated as the total number of animals minus the number of groups, which falls within the recommended range of 10–20, indicating adequate statistical power for this study. Normality and homogeneity of variance were assessed and met prior to ANOVA. Effect sizes and confidence intervals were not calculated.

3. Results

3.1 SPI1 is Markedly Overexpressed in VSMCs Induced by PDGF-BB

We first established a PDGF-BB-induced VSMC IA model and then detected SPI1 expression using RT-qPCR and WB. The findings demonstrated that SPI1 expression levels were higher in the PDGF-BB group than in the control group (Fig. 1A,B). This result suggests that SPI1 may play a role in IA development; however, further studies are required to confirm this.

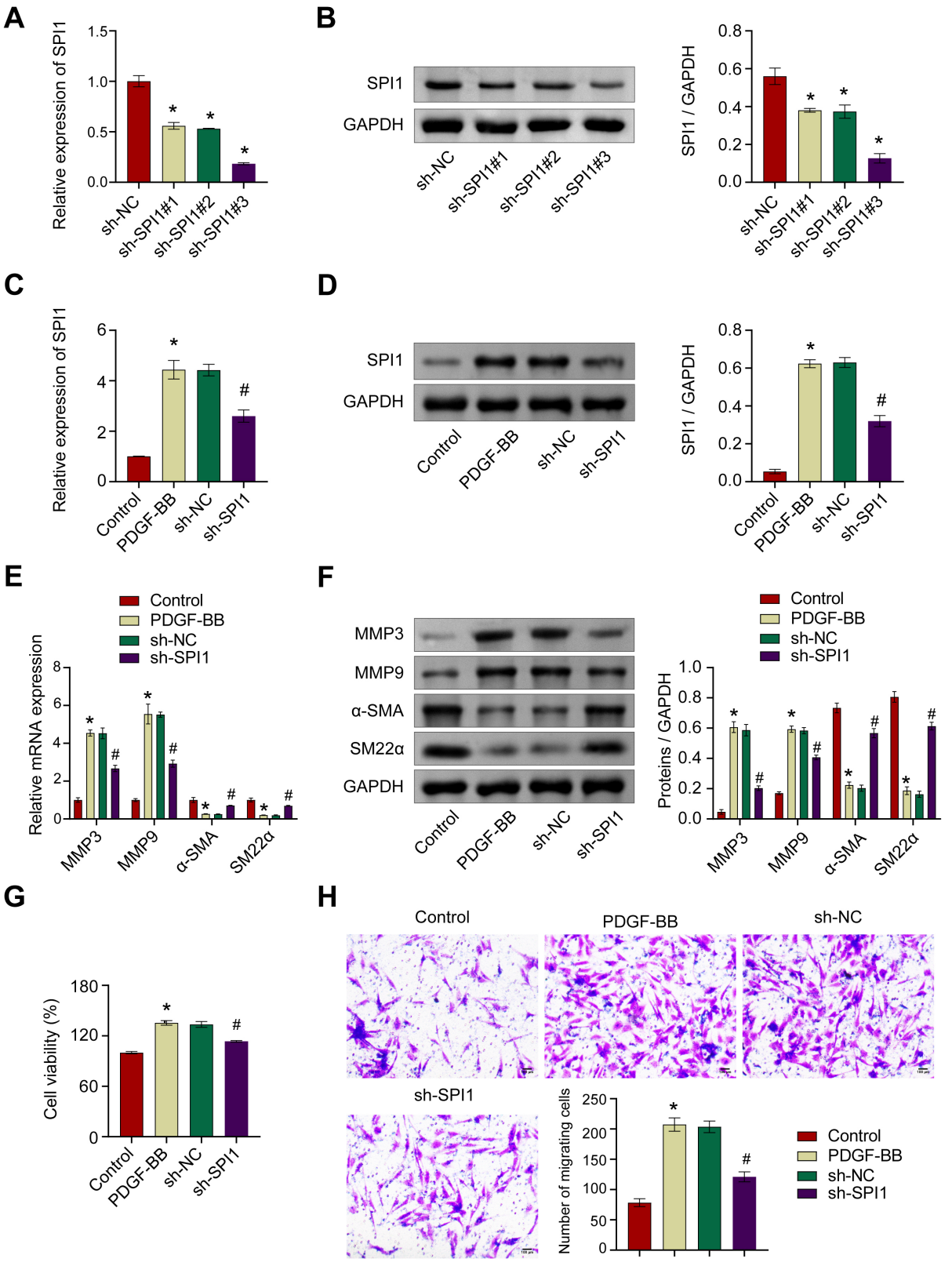

Fig. 2. SPI1 knockdown increases the PDGF-BB-induced change in VSMCs from a synthetic to a contractile phenotype. (A,C) SPI1 expression in VSMCs was examined using RT-qPCR. (B,D) SPI1 expression in VSMCs was examined using WB. (E) The expression of α-SMA, SM22α, MMP3, and MMP9 in VSMCs was examined using RT-qPCR. (F) The expression of α-SMA, SM22α, MMP3, and MMP9 in VSMCs was examined using WB. (G) CCK-8 assay for cell proliferation. (H) Transwell assay for cell migration. Scale bar = 100 μm. n = 3, for Fig. 2A,B: *$p < 0.05$ vs. sh-NC; for Fig. 2C–H: *$p < 0.05$ vs. Control. #$p < 0.05$ vs. sh-NC.

3.2 SPI1 Knockdown Increases the PDGF-BB-induced Change of VSMCs From Synthetic to Contractile Phenotype

To investigate the effect of SPI1 on PDGF-BB-induced VSMCs, we first screened for effective siRNA targets. The results of RT-qPCR and WB assays showed that, compared with the si-NC group, all three targets were able to downregulate SPI1 expression to varying degrees, with si-SPI1#3 showing the most significant knockdown efficiency (Fig. 2A,B). Therefore, it was selected for subsequent experiments. Subsequently, the screened si-SPI1#3 was transfected into VSMCs and grouped for treatment. Both RT-qPCR and WB assays demonstrated that SPI1 expression was downregulated in the sh-SPI1-treated group compared with the sh-NC group, indicating successful transfection of the sh-SPI1 plasmid. SPI1 knockdown efficiency was approximately 41.23% at the mRNA level and 46.67% at the protein level compared with the sh-NC group (Fig. 2C,D). We then measured the levels of contractile smooth muscle cell biomarkers α-SMA and SM22α, as well as synthetic smooth muscle cell biomarkers MMP3 and MMP9, in the cells. RT-qPCR and WB analysis results showed that PDGF-BB treatment reduced α-SMA and SM22α expression and increased MMP3 and MMP9 expression in VSMCs. However, SPI1 knockdown reversed this trend (Fig. 2E,F). In addition, functional experimental results indicated that SPI1 knockdown inhibited PDGF-BB-induced VSMC proliferation (Fig. 2G) and migration ability (Fig. 2H). These results suggest that SPI1 knockdown promotes the conversion of VSMCs from a synthetic phenotype to a contractile phenotype induced by PDGF-BB.

3.3 SPI1 Inhibits Wnt5a Transcription and Activates the Wnt Pathway

To investigate whether SPI1 affects the Wnt pathway in PDGF-BB-induced VSMCs, we used RT-qPCR and WB to detect the expression levels of Wnt5a. The findings demonstrated that Wnt5a levels in VSMCs decreased compared with the Control group after PDGF-BB treatment. Conversely, in PDGF-BB-induced VSMCs, Wnt5a levels increased when SPI1 was knocked down (Fig. 3A,B). In addition, we detected the expression of c-Myc in VSMCs. The findings demonstrated that c-Myc levels increased compared with the Control group after PDGF-BB treatment. However, sh-SPI1 treatment reversed the PDGF-BB-induced increase in c-Myc (Fig. 3B). To further verify the impact of SPI1 on the activity of the canonical Wnt pathway, we examined the nuclear–cytoplasmic distribution of β-catenin. The WB results indicated that PDGF-BB treatment promoted the nuclear translocation of β-catenin, while SPI1 knockdown inhibited the nuclear translocation of β-catenin (Fig. 3C). Meanwhile, the results of the TOP/FOP flash reporter assay showed that SPI1 knockdown significantly reduced the transcriptional activity of β-catenin (Fig. 3D). Next, we predicted the binding of the transcription factor SPI1 to the Wnt5a promoter using the JASPAR website (Fig. 3E). ChIP assays revealed that sh-SPI1 treatment significantly reduced the SPI1 enrichment signal at specific locations (#1, #2, #3) in the Wnt5a promoter region compared with the sh-NC group, demonstrating SPI1 binding to the Wnt5a promoter (Fig. 3F). These data suggest that SPI1 may activate the canonical Wnt pathway by suppressing Wnt5a transcription.

3.4 SPI1 Knockdown Promotes PDGF-BB-induced VSMC Contraction Phenotypic Switching Through Wnt5a

To investigate whether SPI1 promotes PDGF-BB-induced VSMC contractile phenotypic switching through Wnt5a, we introduced the Wnt5a inhibitor Box5. WB results showed that, compared with the sh-NC group, Wnt5a expression was significantly downregulated, whereas β-catenin and c-Myc expression were upregulated after Box5 treatment, while SPI1 expression was almost unaffected. In contrast, SPI1 knockdown upregulated Wnt5a levels and downregulated SPI1, β-catenin, and c-Myc levels. The sh-SPI1+Box5 group reversed the changes in Wnt5a, β-catenin, and c-Myc induced by SPI1 knockdown (Fig. 4A). Although seemingly contradictory, the observation that Wnt5a protein levels were significantly reduced after Box5 treatment is consistent with previous studies in which Box5 also reduced Wnt5a abundance [53,54,55]. We hypothesize that this effect may result from the disruption of a putative positive feedback loop, wherein active Wnt5a signaling normally sustains its own expression. The profound inhibition of downstream signaling by Box5 could thereby lead to transcriptional or translational suppression of Wnt5a, ultimately manifesting as reduced protein levels. Next, we assessed the expression of α-SMA, SM22α, MMP3, and MMP9. Both RT-qPCR and WB results showed that Box5 treatment alone upregulated MMP3 and MMP9 levels and downregulated α-SMA and SM22α levels. In contrast, SPI1 knockdown increased α-SMA and SM22α levels while decreasing MMP3 and MMP9 levels in VSMCs. Similarly, these effects of SPI1 knockdown were reversed when SPI1 knockdown was combined with Box5 treatment (Fig. 4B,C). Furthermore, functional experiments showed that Box5 treatment alone promoted VSMC proliferation and migration, whereas SPI1 knockdown inhibited these functions. Box5 treatment counteracted the inhibitory effects of SPI1 knockdown on cell proliferation and migration (Fig. 4D,E). The rapid phenotypic switching could be related to a swift signaling-mediated mechanism. One possibility is that Box5 interferes with Wnt5a signaling, which may in turn reduce downstream Ca^{2+} flux and lead to immediate cytoskeletal remodeling. This provides a possible explanation for the early functional changes observed within the 2-hour timeframe [56]. Based on the above results, we speculate that SPI1 promotes PDGF-BB-induced VSMC phenotypic switching through Wnt5a.

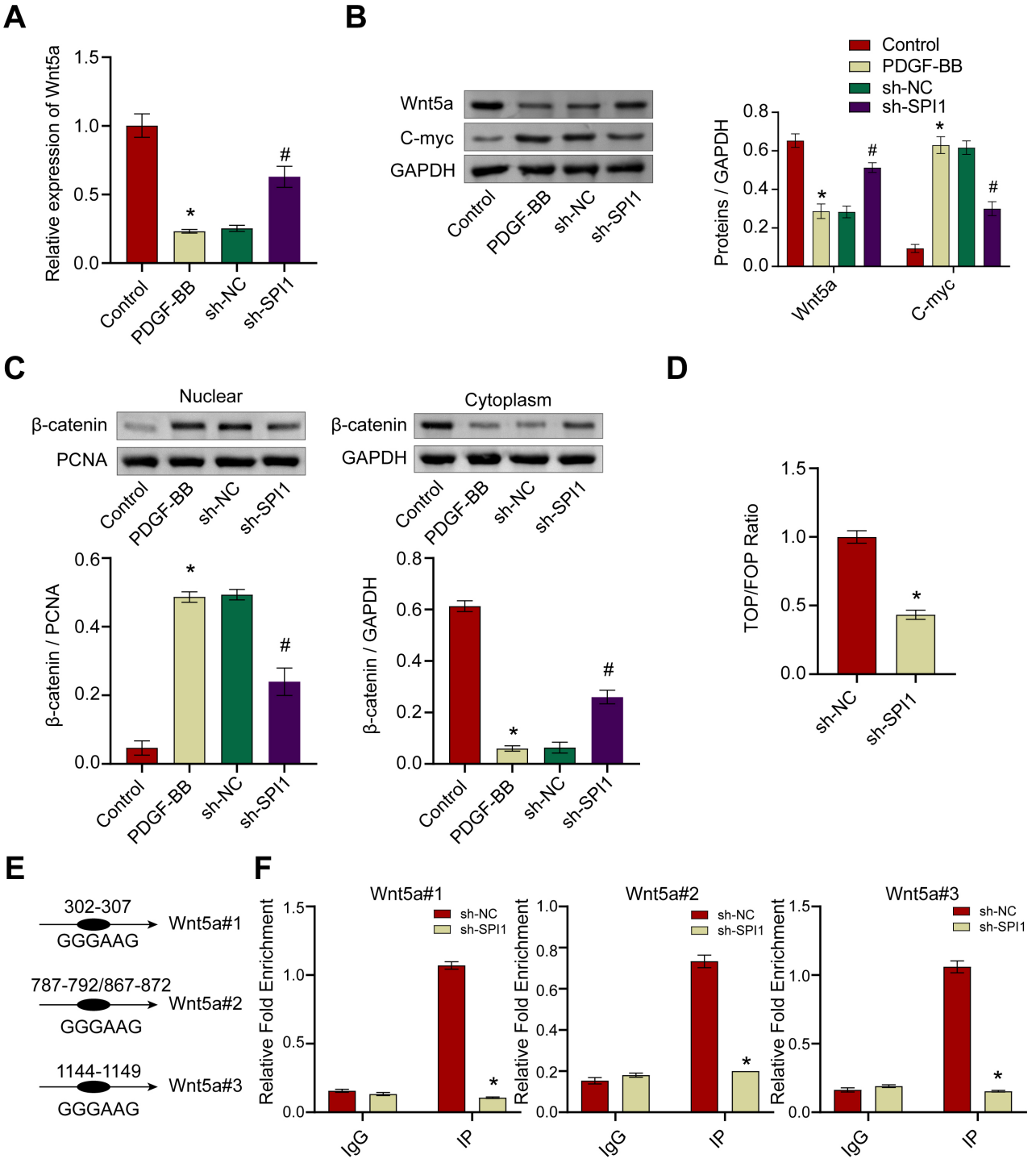

Fig. 3. SPI1 inhibits Wnt5a transcription and activates the Wnt pathway. (A) Wnt5a expression in VSMCs was examined using RT-qPCR. (B) Wnt5a and c-Myc expression in VSMCs was examined using WB. (C) WB detection of β-catenin expression in the nucleus and cytoplasm. (D) TOP/FOP flash reporter assay for transcriptional activity. (E) Prediction of SPI1 binding sites in the Wnt5a promoter using JASPAR. (F) ChIP assay confirming SPI1 binding to the Wnt5a promoter. n = 3, *$p < 0.05$ vs. Control. #$p < 0.05$ vs. sh-NC. ChIP, Chromatin immunoprecipitation.

3.5 SPI1 Knockdown Inhibits IA Development and Progression in the Mouse Model

We first established an IA mouse model to investigate how SPI1 influences the formation and development of IA. HE staining results showed that IA mice exhibited vascular dilatation and fracture of elastic fibers in the middle layer, whereas the control group showed no such changes. SPI1 knockdown significantly attenuated these changes (Fig. 5A). Further quantitative analysis of aneurysm size showed that aneurysm size was significantly increased in

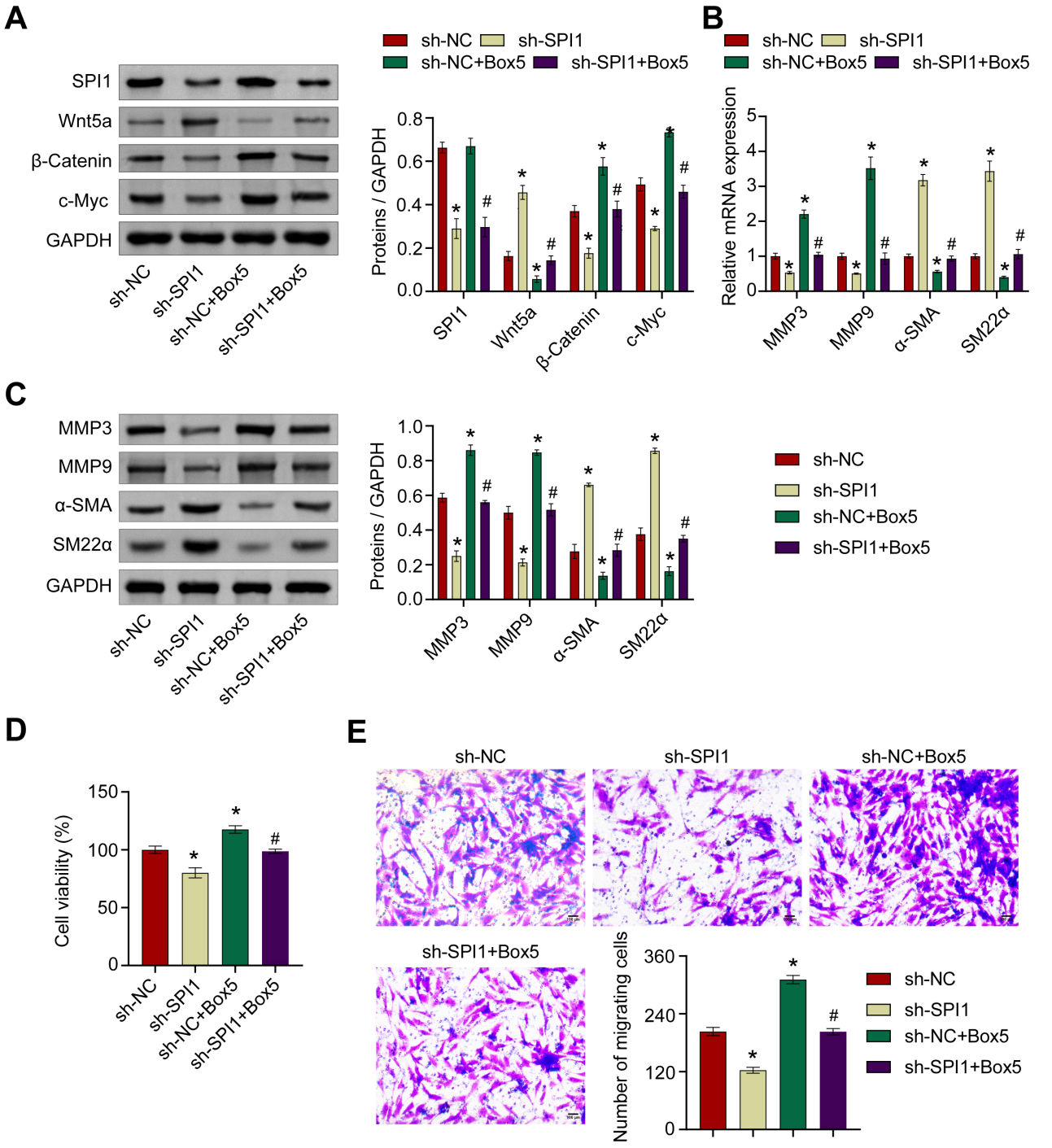

Fig. 4. SPI1 knockdown promotes PDGF-BB-induced VSMC contractile phenotypic switching through Wnt5a. (A) Analysis of SPI1, Wnt5a, β-Catenin, and c-Myc expression in VSMCs using WB. (B) The expression of α-SMA, SM22α, MMP3, and MMP9 in VSMCs was assessed by RT-qPCR. (C) The expression of α-SMA, SM22α, MMP3, and MMP9 in VSMCs using WB. (D) CCK-8 assay for cell proliferation. (E) Transwell assay to detect cell migration. Scale bar = 100 μm. n = 3, *$p < 0.05$ vs. sh-NC. #$p < 0.05$ vs. sh-SPI1.

the IA group and the sh-NC group, whereas significantly decreased in the sh-SPI1 group (Fig. 5A). Victoria Blue staining showed disrupted elastic fibers and reduced elastic fiber content in the cerebral arterial ring of IA mice. In contrast, the sh-SPI1 group exhibited elastic fiber morphology and staining intensity similar to those of the control group (Fig. 5B). RT-qPCR analysis demonstrated that SPI1 expression was significantly downregulated in the sh-SPI1 group, while Wnt5a levels were increased (Fig. 5C). WB analysis further confirmed that SPI1 knockdown promoted Wnt5a expression while downregulating β-catenin and c-Myc expression (Fig. 5D). In addition, IHC results showed that SPI1 was highly expressed in vascular smooth muscle cells of diseased vessels compared with the Control

group, and the positive rate of SPI1 decreased after transfection with the sh-SPI1 plasmid, indicating that the protective effect of SPI1 knockdown may act directly on vascular smooth muscle cells in the diseased area (Fig. 5E). Next, we examined the effects of SPI1 on the expression of SM22α, α-SMA, MMP3, and MMP9 in the cerebral arterial ring. Both RT-qPCR and WB results showed that the expression levels of SM22α and α-SMA were reduced, whereas those of MMP3 and MMP9 were increased in the arterial rings of IA mice. SPI1 knockdown increased the expression of SM22α and α-SMA in the arterial rings of IA mice, while the expression levels of MMP3 and MMP9 were decreased (Fig. 5F,G). Lastly, we used ELISA to examine the regulatory effects of SPI1 on inflammatory responses in the cerebral arterial ring. The findings demonstrated that the expression levels of the pro-inflammatory factors IL-6, IL-1β, and TNF-α were increased compared with the Control group, whereas the expression level of the anti-inflammatory factor IL-10 was decreased in the IA group (Fig. 5H). SPI1 knockdown reversed these inflammatory changes in the IA group. These results suggest that SPI1 knockdown can effectively inhibit the formation and progression of IA.

4. Discussion

It has been demonstrated that SPI1, a cancer gene selectively activated in acute mouse erythroleukemia induced by the Friend spleen focus-forming virus (SFFV) [22], is associated with disease development in several malignant tumors. For instance, SPI1 regulates HK2 involvement in the pathophysiology of malignant melanoma via the AKT1/MTOR pathway [23]. SPI1 has also been identified as a key transcriptional activator of SNHG6, which promotes oncogenesis by sequestering miR-485-3p, thereby delineating a critical SPI1-driven oncogenic pathway in lung cancer [57]. In addition, SPI1 promotes the migration and tubulogenesis of endothelial cells by upregulating VEGFA, underscoring its pivotal role in angiogenesis [58]. In the context of stroke, the long non-coding RNA FTX functions as a molecular sponge for miR-342-3p, thereby upregulating the expression of the transcription factor SPI1. This FTX/miR-342-3p/SPI1 axis has been shown to promote angiogenesis in brain microvascular endothelial cells [59]. Overall, existing evidence indicates that SPI1 contributes to the development of several malignancies and also plays a role in vascular biology. Our study suggests that SPI1 facilitates IA formation, which is consistent with previous findings. SPI1 knockdown promotes the conversion of vascular smooth muscle cells from a synthetic to a contractile phenotype in IA, while also preventing vascular wall thickening and the loss of elastic fibers. Furthermore, SPI1 knockdown reduces inflammatory responses. These findings suggest that SPI1 may play a pathogenic role in IA.

The loss and degenerative changes of vascular smooth muscle cells are the main histopathological features of IA [16]. In response to environmental stimuli, vascular smooth muscle cells can undergo phenotypic switching from a contractile state to a pro-inflammatory and synthetic state, and this process is crucial to IA degeneration and rupture [60]. In the present study, SPI1 knockdown upregulated the expression of contractile markers (α-SMA and SM22α) and downregulated the expression of synthetic markers (MMP3 and MMP9) *in vitro*. These findings were further validated *in vivo*. Together, these results indicate that inhibition of SPI1 promotes the phenotypic transition of vascular smooth muscle cells from a synthetic phenotype to a contractile phenotype. These results further underscore the critical role of SPI1 in IA pathogenesis and suggest that it may serve as a potential therapeutic target.

SPI1 is a transcription factor that has been shown to reduce FTO transcriptional activity and promote glioblastoma growth by controlling the processing of PRI-MIR-10A via M6A-dependent pathways [24]. Our findings show that SPI1 can specifically bind to the Wnt5a promoter region and suppress transcription. Knockdown of SPI1 increased Wnt5a expression in VSMCs. Wnt5a, an important member of the Wnt protein family, plays an essential role in embryonic development by regulating fundamental cellular processes, including proliferation, differentiation, apoptosis, and migration, influencing cell fate determination and polarity [61]. Wnt5a can activate the Hippo pathway through ROR2 signaling to inhibit YAP1 activity and melanoma growth [62]. The non-canonical Wnt and β-catenin signaling pathways are mutually antagonistic and often exert reciprocal effects on each other [63]. By attaching to the Ror2 receptor, Wnt5a can effectively inhibit the canonical β-catenin/TCF signaling cascade induced by Wnt3a [64]. Wnt5a signaling also inhibits β-catenin activity, as well as the expression of LGR5, RSPO3, and VEGFA, thereby suppressing colon cancer cell stemness [65]. Moreover, accumulating evidence highlights the critical role of the canonical Wnt/β-catenin pathway in regulating the phenotypic switching of VSMCs toward a synthetic phenotype. For instance, Lyon et al. [66] described its role in promoting VSMC proliferation, which is a key feature of this transition. In addition, studies on E2F5 and by Rong et al. [67] showed that interventions that inhibit Wnt/β-catenin signaling, such as E2F5 downregulation or SLC6A6 overexpression, can maintain the contractile phenotype and reduce pathological vascular remodeling [68]. Previous research has also shown that Wnt5a can regulate the phenotypic switching of vascular smooth muscle cells and thereby inhibit IA progression [46]. In our study, inhibition of Wnt5a reversed the effects of SPI1 knockdown on the synthetic-to-contractile phenotypic switching of VSMCs and increased β-catenin expression. These findings suggest that SPI1 may regulate the synthetic-contractile phenotypic switching of VSMCs by inhibiting Wnt5a transcription and activating canonical

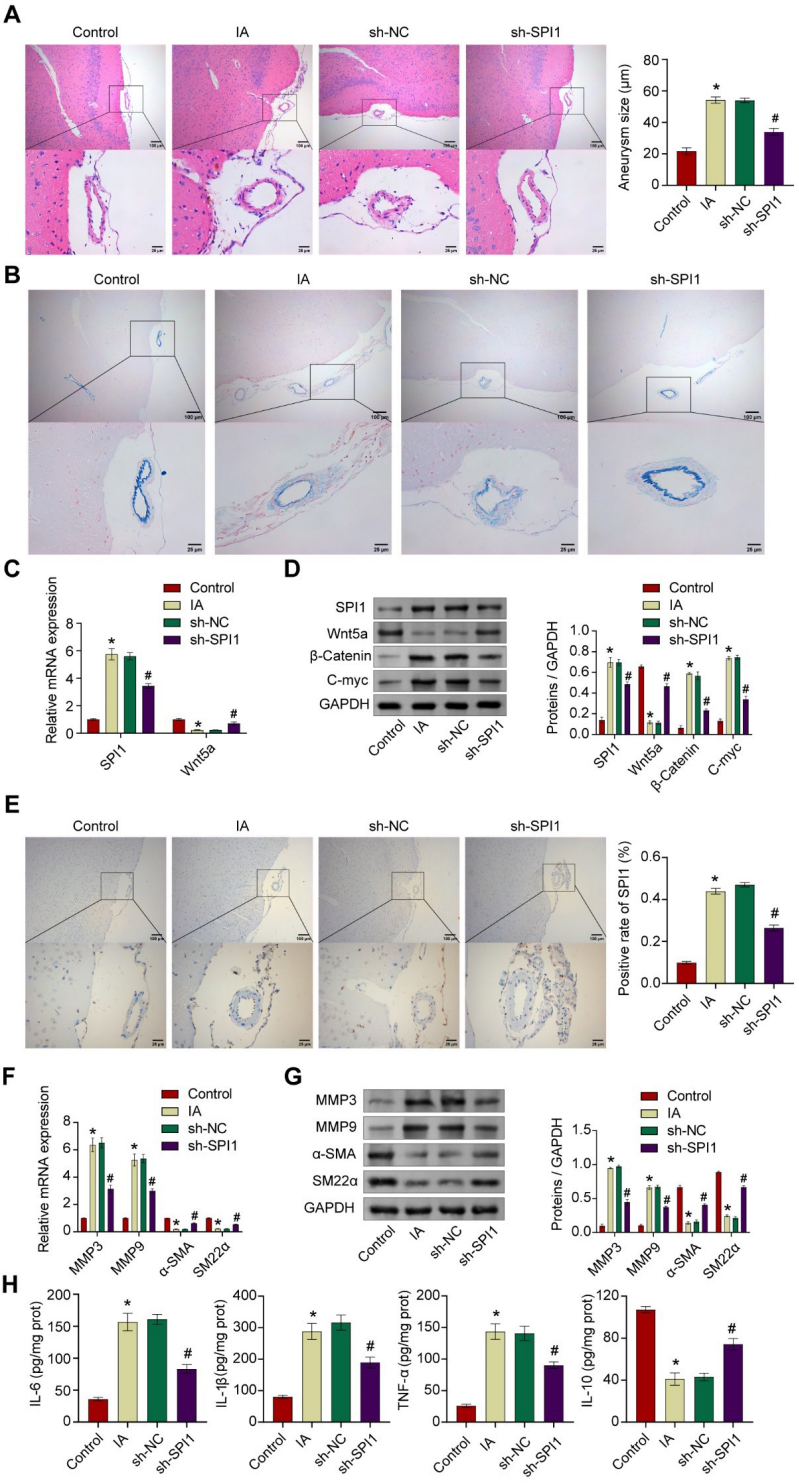

Fig. 5. SPI1 knockdown inhibits IA development and progression in the mouse model. (A) HE staining was used to assess morphological changes in the circle of Willis, and aneurysm size was quantitatively analyzed. Upper: Scale bar = 100 μm; Lower: scale bar = 25 μm. (B) Elastic fibers in the cerebral arterial ring were evaluated by Victoria Blue staining. Upper: Scale bar = 100 μm; Lower: scale bar = 25 μm. (C) RT-qPCR was used to detect the expression of SPI1 and Wnt5a. (D) WB was used to detect the expression of β-catenin, c-Myc, Wnt5a, and SPI1. (E) IHC was used to detect SPI1 expression in the smooth muscle layer of the IA model. Upper: Scale bar = 100 μm; Lower: scale bar = 25 μm. (F) The expression of MMP3, MMP9, α-SMA, and SM22α in the cerebral arterial ring was examined by RT-qPCR. (G) The expression of MMP3, MMP9, α-SMA, and SM22α in the cerebral arterial ring was examined by WB. (H) The expression levels of IL-6, IL-1β, TNF-α, and IL-10 in the cerebral arterial ring were detected by ELISA. n = 6, *$p < 0.05$ vs. Control. #$p < 0.05$ vs. sh-NC. IA, intracranial aneurysm; HE, hematoxylin and eosin; IHC, immunohistochemistry.

Wnt signaling, thereby influencing IA development. To our knowledge, this study provides new insights into the role of the SPI1/Wnt5a signaling axis in regulating Wnt signaling during IA progression.

5. Limitations

Several limitations should be acknowledged. First, activation of the canonical Wnt pathway was primarily inferred from the expression levels of β-catenin and c-Myc. During revision, we further performed nuclear β-catenin localization analysis, which confirmed that SPI1 knockdown inhibits β-catenin nuclear translocation and thus provides more direct evidence. However, deeper causal validation, such as rescue experiments using a β-catenin pathway inhibitor, is still lacking and warrants further investigation. Second, the reduction in Wnt5a protein levels following Box5 treatment complicated the interpretation of the rescue experiments, and the proposed positive feedback loop hypothesis remains speculative. Further studies examining Wnt5a transcriptional changes or protein stability are therefore needed. Third, although we supplemented the study with functional assays assessing cell proliferation and migration, the effects of SPI1 on VSMC contractility and apoptosis remain unexplored. Future studies incorporating these functional assessments would further clarify the biological consequences of SPI1-mediated phenotypic switching. Finally, the broader regulatory network of SPI1, as well as its upstream and downstream molecular mechanisms in IA pathogenesis, remains to be fully elucidated. Future studies with larger sample sizes, additional functional assays, and more comprehensive measurements of pathway activity are warranted to further validate the role of the SPI1/Wnt5a/β-catenin signaling axis in IA progression.

6. Conclusions

This study provides preliminary evidence that SPI1 is significantly overexpressed in experimental IA models and may suppress the transcription of Wnt5a by directly binding to its promoter, thereby promoting activation of the typical Wnt/β-catenin pathway, which may drive VSMCs toward a synthetic phenotype and contribute to IA formation. *In vivo* experiments further suggest that SPI1 knockdown is associated with reduced vascular wall thickening, elastic fiber destruction, and inflammatory responses in the IA mouse model. Functional experiments showed that SPI1 knockdown may inhibit the proliferation and migration of VSMCs. In addition, nuclear β-catenin localization and TOP/FOP assays are consistent with a regulatory effect of the classical Wnt pathway by SPI1. These findings suggest potential novel molecular targets and therapeutic strategies for IA.

Abbreviations

IA, Intracranial aneurysm; VSMCs, vascular smooth muscle cells; MMPs, matrix metalloproteinases; SPI1, Spi-1 Proto-Oncogene; ETS, E26 transformation-specific; NMT1, N-myristoyltransferase 1; PI3K/AKT/mTOR, Phosphoinositide 3-kinase/Protein Kinase B/Mammalian Target of Rapamycin; TLR4/NF-κB, toll-like receptor 4/nuclear factor-κB; GEO, Gene Expression Omnibus; Wnt, Wingless/Integrated; PCP, planar cell polarity; BTK, Bruton's tyrosine kinase; ERK1/2, Extracellular signal-regulated kinase 1/2; ROR1/DOCK2, Receptor Tyrosine Kinase Like Orphan Receptor 1/Dedicator of cytokinesis 2; ABCA1, ATP-binding cassette transporter A1; CTHRC1, collagen triple helix repeat containing-1; FBS, fetal bovine serum; PDGF-BB, Platelet-Derived Growth Factor BB; GAPDH, glyceraldehyde-3-phosphate dehydrogenase; ECL, Enhanced Chemiluminescence; TNF-α, tumor necrosis factor-α; IL-1β, interleukin-1β; IL-6, interleukin-6; IL-10, interleukin-10; OD, Optical Density; DAB, 3,3'-diaminobenzidine; α-SMA, α-smooth muscle actin; SM22α, smooth muscle 22α; MMP3, matrix metallopeptidase 3; MMP9, matrix metallopeptidase 9; SFFV, spleen focus-forming virus; HK2, hexokinase 2; SNHG6, small nucleolar RNA host gene 6; VEGFA, Vascular Endothelial Growth Factor A; FTX, five prime to Xist; FTO, Fat Mass and Obesity-associated Protein; M6A, N6-methyladenosine; YAP1, Yes1 associated transcriptional regulator; E2F5, E2F transcription factor 5; SLC6A6, Solute Carrier Family 6 Member 6.

Availability of Data and Materials

The datasets generated during and analysed during the current study are not publicly available but are available from the corresponding author on reasonable request.

Author Contributions

ZSL and YW designed the research study. WCW and WL performed the research. JP and JXL collected and analyzed the data. ZSL wrote the manuscript. YW provided supervision, guidance, and critical revision of the manuscript. All authors contributed to editorial changes in the manuscript. All authors read and approved the final manuscript. All authors have participated sufficiently in the work and agreed to be accountable for all aspects of the work.

Ethics Approval and Consent to Participate

Ethical approval was granted by the Ethics Committee of Changsha First Hospital (Number: 2023-62). All animal experiments in this study were followed by the ARRIVE guidelines and approved by Changsha First Hospital. All procedures also adhered to the 3Rs principle (Replacement, Reduction, Refinement), in accordance with the Guidelines for Ethical Review of Laboratory Animal Welfare (GB/T 35892-2018).

Acknowledgment

Not applicable.

Funding

This research received no external funding.

Conflicts of Interest

The authors declare no conflicts of interest.

Declaration of AI and AI-Assisted Technologies in the Writing Process

During the preparation of this work, the authors used DeepSeek to check language expression and perform grammatical polishing. After using this tool, the authors reviewed and edited the content as needed and take full responsibility for the content of the publication. The authors confirm that AI tools were not used in other stages of the research, such as study design, literature search, or data analysis.

Supplementary Material

Supplementary material associated with this article can be found, in the online version, at https://doi.org/10.31083/FBL49794.

References

[1] Nafees Ahmed S, Prakasam P. A systematic review on intracranial aneurysm and hemorrhage detection using machine learning and deep learning techniques. Progress in Biophysics and Molecular Biology. 2023; 183: 1–16. https://doi.org/10.1016/j.pbiomolbio.2023.07.001

[2] Glavan M, Jelic A, Levard D, Frösen J, Keränen S, Franx BAA, et al. CNS-associated macrophages contribute to intracerebral aneurysm pathophysiology. Acta Neuropathologica Communications. 2024; 12: 43. https://doi.org/10.1186/s40478-024-01756-5

[3] Yin Z, Zhang Q, Zhao Y, Lu J, Ge P, Xie H, et al. Prevalence and Procedural Risk of Intracranial Atherosclerotic Stenosis Coexisting With Unruptured Intracranial Aneurysm. Stroke. 2023; 54: 1484–1493. https://doi.org/10.1161/STROKEAHA.122.041553

[4] Matsushiro M, Harada D, Ueyama K, Kashiwagi H, Ishiura Y, Yamada H, et al. Intracranial aneurysm as a possible complication of osteogenesis imperfecta: a case series and literature review. Endocrine Journal. 2023; 70: 697–702. https://doi.org/10.1507/endocrj.EJ22-0620

[5] Levinson S, Pendharkar AV, Gauden AJ, Heit JJ. Modern Imaging of Aneurysmal Subarachnoid Hemorrhage. Radiologic Clinics of North America. 2023; 61: 457–465. https://doi.org/10.1016/j.rcl.2023.01.004

[6] Chung DY, Abdalkader M, Nguyen TN. Aneurysmal Subarachnoid Hemorrhage. Neurologic Clinics. 2021; 39: 419–442. https://doi.org/10.1016/j.ncl.2021.02.006

[7] Lauzier DC, Jayaraman K, Yuan JY, Diwan D, Vellimana AK, Osbun JW, et al. Early Brain Injury After Subarachnoid Hemorrhage: Incidence and Mechanisms. Stroke. 2023; 54: 1426–1440. https://doi.org/10.1161/STROKEAHA.122.040072

[8] Wan X, Wu X, Kang J, Fang L, Tang Y. Prognostic model for aneurysmal subarachnoid hemorrhage patients requiring mechanical ventilation. Annals of Clinical and Translational Neurology. 2023; 10: 1569–1577. https://doi.org/10.1002/acn3.51846

[9] Yan Y, Xiong J, Xu F, Wang C, Zeng Z, Tang H, et al. SDF-1α/CXCR4 Pathway Mediates Hemodynamics-Induced Formation of Intracranial Aneurysm by Modulating the Phenotypic Transformation of Vascular Smooth Muscle Cells. Translational Stroke Research. 2022; 13: 276–286. https://doi.org/10.1007/s12975-021-00925-1

[10] Wang K, Tan G, Tian R, Zhou H, Xiang C, Pan K. Circular RNA circ_0021001 regulates miR-148b-3p/GREM1 axis to modulate proliferation and apoptosis of vascular smooth muscle cells. Metabolic Brain Disease. 2022; 37: 2027–2038. https://doi.org/10.1007/s11011-022-01014-4

[11] Wei H, Wang G, Tian Q, Liu C, Han W, Wang J, et al. Low shear stress induces macrophage infiltration and aggravates aneurysm wall inflammation via CCL7/CCR1/TAK1/ NF-κB axis. Cellular Signalling. 2024; 117: 111122. https://doi.org/10.1016/j.cellsig.2024.111122

[12] Duan J, Zhao Q, He Z, Tang S, Duan J, Xing W. Current understanding of macrophages in intracranial aneurysm: relevant etiological manifestations, signaling modulation and therapeutic strategies. Frontiers in Immunology. 2024; 14: 1320098. https://doi.org/10.3389/fimmu.2023.1320098

[13] Fan H, Tian H, Jin F, Zhang X, Su S, Liu Y, et al. CypD induced ROS output promotes intracranial aneurysm formation and rupture by 8-OHdG/NLRP3/MMP9 pathway. Redox Biology. 2023; 67: 102887. https://doi.org/10.1016/j.redox.2023.102887

[14] Li S, Shi Y, Liu P, Song Y, Liu Y, Ying L, et al. Metformin inhibits intracranial aneurysm formation and progression by regulating vascular smooth muscle cell phenotype switching via the AMPK/ACC pathway. Journal of Neuroinflammation. 2020; 17: 191. https://doi.org/10.1186/s12974-020-01868-4

[15] Shi Y, Li S, Song Y, Liu P, Yang Z, Liu Y, et al. Nrf-2 signaling inhibits intracranial aneurysm formation and progression by modulating vascular smooth muscle cell phenotype and function. Journal of Neuroinflammation. 2019; 16: 185. https://doi.org/10.1186/s12974-019-1568-3

[16] Oka M, Shimo S, Ohno N, Imai H, Abekura Y, Koseki H, et al. Dedifferentiation of smooth muscle cells in intracranial aneurysms and its potential contribution to the pathogenesis. Scientific Reports. 2020; 10: 8330. https://doi.org/10.1038/s41598-020-65361-x

[17] Wei L, Yang C, Wang G, Li K, Zhang Y, Guan H, et al. Interleukin Enhancer Binding Factor 2 Regulates Cell Viability and Apoptosis of Human Brain Vascular Smooth Muscle Cells. Journal of Molecular Neuroscience : MN. 2021; 71: 225–233. https://doi.org/10.1007/s12031-020-01638-0

[18] Wang C, Luo Y, Tang H, Yan Y, Chang X, Zhao R, et al. Hsa_circ_0031608: A Potential Modulator of VSMC Phenotype in the Rupture of Intracranial Aneurysms. Frontiers in Molecular Neuroscience. 2022; 15: 842865. https://doi.org/10.3389/fnmol.2022.842865

[19] Li G, Hao W, Hu W. Transcription factor PU.1 and immune cell differentiation (Review). International Journal of Molecular Medicine. 2020; 46: 1943–1950. https://doi.org/10.3892/ijmm.2020.4763

[20] Fang Y, Chen W, Li Z, Chen Y, Wu X, Zhu X, et al. The role of a key transcription factor PU.1 in autoimmune diseases. Frontiers in Immunology. 2022; 13: 1001201. https://doi.org/10.3389/fimmu.2022.1001201

[21] Nguyen VC, Ray D, Gross MS, de Tand MF, Frézal J, Moreau-Gachelin F. Localization of the human oncogene SPI1 on chromosome 11, region p11.22. Human Genetics. 1990; 84: 542–546. https://doi.org/10.1007/BF00210807

[22] Wu J, Zhu S, Lin R, Cai W, Lin H, Wu J, et al. LINC00887 regulates malignant progression and T-cell chemotaxis in clear cell renal cell carcinoma by activating CD70 via recruitment of SPI1. Gene. 2024; 893: 147910. https://doi.org/10.1016/j.gene.2023.147910

[23] Liu C, Qiu X, Gao J, Gong Z, Zhou X, Luo H, et al. SPI1 in-

volvement in malignant melanoma pathogenesis by regulation of HK2 through the AKT1/mTOR pathway. Journal of Cellular and Molecular Medicine. 2023; 27: 2675–2683. https://doi.org/10.1111/jcmm.17844

[24] Zhang S, Zhao S, Qi Y, Li B, Wang H, Pan Z, et al. SPI1-induced downregulation of FTO promotes GBM progression by regulating pri-miR-10a processing in an m6A-dependent manner. Molecular Therapy. Nucleic Acids. 2022; 27: 699–717. https://doi.org/10.1016/j.omtn.2021.12.035

[25] Qiu P, Li X, Gong M, Wen P, Wen J, Xu L, et al. SPI1 Mediates N-Myristoyltransferase 1 to Advance Gastric Cancer Progression via PI3K/AKT/mTOR Pathway. Canadian Journal of Gastroenterology & Hepatology. 2023; 2023: 2021515. https://doi.org/10.1155/2023/2021515

[26] Gao J, Dai C, Yu X, Yin XB, Zhou F. Long noncoding RNA LINC00324 exerts protumorigenic effects on liver cancer stem cells by upregulating fas ligand via PU box binding protein. FASEB Journal : Official Publication of the Federation of American Societies for Experimental Biology. 2020; 34: 5800–5817. https://doi.org/10.1096/fj.201902705RR

[27] Qu K, Mo S, Huang J, Liu S, Zhang S, Shen J, et al. SPI1-KLF1/LYL1 axis regulates lineage commitment during endothelial-to-hematopoietic transition from human pluripotent stem cells. iScience. 2024; 27: 110409. https://doi.org/10.1016/j.isci.2024.110409

[28] Zheng PF, Zou QC, Chen LZ, Liu P, Liu ZY, Pan HW. Identifying patterns of immune related cells and genes in the peripheral blood of acute myocardial infarction patients using a small cohort. Journal of Translational Medicine. 2022; 20: 321. https://doi.org/10.1186/s12967-022-03517-1

[29] Liu Z, Huang S. Upregulation of SPI1 during myocardial infarction aggravates cardiac tissue injury and disease progression through activation of the TLR4/NFκB axis. American Journal of Translational Research. 2022; 14: 2709–2727.

[30] Das D, Podder S. Unraveling the molecular crosstalk between Atherosclerosis and COVID-19 comorbidity. Computers in Biology and Medicine. 2021; 134: 104459. https://doi.org/10.1016/j.compbiomed.2021.104459

[31] Zhang Q, Liu H, Zhang M, Liu F, Liu T. Identification of co-expressed central genes and transcription factors in atherosclerosis-related intracranial aneurysm. Frontiers in Neurology. 2023; 14: 1055456. https://doi.org/10.3389/fneur.2023.1055456

[32] Yu XH, Guo XN, Li K, Li JW, Wang K, Wang D, et al. The Role of Wnt5a in Inflammatory Diseases. Immunology. 2025; 174: 203–212. https://doi.org/10.1111/imm.13882

[33] Wang X, Xin H, Ning X, Zhang Y, Liu F, Zhang Z, et al. Strontium-loaded titanium implant with rough surface modulates osseointegration by changing sfrp4 in canonical and non-canonical Wnt signaling pathways. Biomedical Materials (Bristol, England). 2022; 17: 10.1088/1748–605X/ac61fb. https://doi.org/10.1088/1748-605X/ac61fb

[34] Rogers S, Scholpp S. Vertebrate Wnt5a - At the crossroads of cellular signalling. Seminars in Cell & Developmental Biology. 2022; 125: 3–10. https://doi.org/10.1016/j.semcdb.2021.10.002

[35] Xue C, Chu Q, Shi Q, Zeng Y, Lu J, Li L. Wnt signaling pathways in biology and disease: mechanisms and therapeutic advances. Signal Transduction and Targeted Therapy. 2025; 10: 106. https://doi.org/10.1038/s41392-025-02142-w

[36] Liu Q, Yang C, Wang S, Shi D, Wei C, Song J, et al. Wnt5a-induced M2 polarization of tumor-associated macrophages via IL-10 promotes colorectal cancer progression. Cell Communication and Signaling : CCS. 2020; 18: 51. https://doi.org/10.1186/s12964-020-00557-2

[37] Bueno MLP, Saad STO, Roversi FM. WNT5A in tumor development and progression: A comprehensive review. Biomedicine & Pharmacotherapy = Biomedecine & Pharmacotherapie. 2022; 155: 113599. https://doi.org/10.1016/j.biopha.2022.113599

[38] Asem MS, Buechler S, Wates RB, Miller DL, Stack MS. Wnt5a Signaling in Cancer. Cancers. 2016; 8: 79. https://doi.org/10.3390/cancers8090079

[39] Guo R, Xing QS. Roles of Wnt Signaling Pathway and ROR2 Receptor in Embryonic Development: An Update Review Article. Epigenetics Insights. 2022; 15: 25168657211064232. https://doi.org/10.1177/25168657211064232

[40] Astudillo P. Wnt5a Signaling in Gastric Cancer. Frontiers in Cell and Developmental Biology. 2020; 8: 110. https://doi.org/10.3389/fcell.2020.00110

[41] Brandenburg J, Reiling N. The Wnt Blows: On the Functional Role of Wnt Signaling in Mycobacterium tuberculosis Infection and Beyond. Frontiers in Immunology. 2016; 7: 635. https://doi.org/10.3389/fimmu.2016.00635

[42] Zeng R, Huang J, Zhong MZ, Li L, Yang G, Liu L, et al. Multiple Roles of WNT5A in Breast Cancer. Medical Science Monitor : International Medical Journal of Experimental and Clinical Research. 2016; 22: 5058–5067. https://doi.org/10.12659/msm.902022

[43] Pashirzad M, Sathyapalan T, Sahebkar A. Clinical Importance of Wnt5a in the Pathogenesis of Colorectal Cancer. Journal of Oncology. 2021; 2021: 3136508. https://doi.org/10.1155/2021/3136508

[44] Hasan MK, Ghia EM, Rassenti LZ, Widhopf GF, Kipps TJ. Wnt5a enhances proliferation of chronic lymphocytic leukemia and ERK1/2 phosphorylation via a ROR1/DOCK2-dependent mechanism. Leukemia. 2021; 35: 1621–1630. https://doi.org/10.1038/s41375-020-01055-7

[45] Wang D, Zhang Y, Ye T, Zhang R, Zhang L, Shi D, et al. Cthrc1 deficiency aggravates wound healing and promotes cardiac rupture after myocardial infarction via non-canonical WNT5A signaling pathway. International Journal of Biological Sciences. 2023; 19: 1299–1315. https://doi.org/10.7150/ijbs.79260

[46] Li Z, Huang J, Yang L, Li X, Li W. WNTA5-mediated miR-374a-5p regulates vascular smooth muscle cell phenotype transformation and M1 macrophage polarization impacting intracranial aneurysm progression. Scientific Reports. 2024; 14: 559. https://doi.org/10.1038/s41598-024-51243-z

[47] Ackers I, Szymanski C, Silver MJ, Malgor R. Oxidized Low-Density Lipoprotein Induces WNT5A Signaling Activation in THP-1 Derived Macrophages and a Human Aortic Vascular Smooth Muscle Cell Line. Frontiers in Cardiovascular Medicine. 2020; 7: 567837. https://doi.org/10.3389/fcvm.2020.567837

[48] Li X, Wen J, Dong Y, Zhang Q, Guan J, Liu F, et al. Wnt5a promotes renal tubular inflammation in diabetic nephropathy by binding to CD146 through noncanonical Wnt signaling. Cell Death & Disease. 2021; 12: 92. https://doi.org/10.1038/s41419-020-03377-x

[49] Dang DNP, Kamio Y, Kawakatsu T, Makino H, Hokamura K, Imai R, et al. Protective Effect of Resveratrol Against Intracranial Aneurysm Rupture in Mice. Journal of Neuroscience Research. 2025; 103: e70059. https://doi.org/10.1002/jnr.70059

[50] American Veterinary Medical Association. AVMA Guidelines for the Euthanasia of Animals: 2020 Edition. 2020. Available at: https://www.avma.org/resources-tools/avma-policies/avma-guidelines-euthanasia-animals (Accessed: 26 May 2026).

[51] Song C, Zhang K, Luo C, Zhao X, Xu B. Inhibiting the NF-κB/DRP1 Axis Affords Neuroprotection after Spinal Cord Injury via Inhibiting Polarization of Pro-Inflammatory Microglia. Frontiers in Bioscience (Landmark Edition). 2024; 29: 307. https://doi.org/10.31083/j.fbl2908307

[52] Yokosuka K, Rutledge C, Kamio Y, Kuwabara A, Sato H, Rahmani R, et al. Roles of Phytoestrogen in the Pathophysiology of Intracranial Aneurysm. Stroke. 2021; 52: 2661–2670. https://doi.org/10.1161/STROKEAHA.120.032042

[53] Zou W, Wang X, Sun R, Hu J, Ye D, Bai G, et al. PM2.5 Induces Airway Remodeling in Chronic Obstructive Pulmonary Diseases via the Wnt5a/β-Catenin Pathway. International Journal of Chronic Obstructive Pulmonary Disease. 2021; 16: 3285–3295. https://doi.org/10.2147/COPD.S334439

[54] Zuo X, Liu Z, Ma J, Ding Y, Cai S, Wu C, et al. Wnt 5a mediated inflammatory injury of renal tubular epithelial cells dependent on calcium signaling pathway in Trichloroethylene sensitized mice. Ecotoxicology and Environmental Safety. 2022; 243: 114019. https://doi.org/10.1016/j.ecoenv.2022.114019

[55] Wu T, Zhang J, Geng M, Tang SJ, Zhang W, Shu J. Nucleoside reverse transcriptase inhibitors (NRTIs) induce proinflammatory cytokines in the CNS via Wnt5a signaling. Scientific Reports. 2017; 7: 4117. https://doi.org/10.1038/s41598-017-03446-w

[56] Sun G, Wu L, Sun G, Shi X, Cao H, Tang W. WNT5a in Colorectal Cancer: Research Progress and Challenges. Cancer Management and Research. 2021; 13: 2483–2498. https://doi.org/10.2147/CMAR.S289819

[57] Gao N, Ye B. SPI1-induced upregulation of lncRNA SNHG6 promotes non-small cell lung cancer via miR-485-3p/VPS45 axis. Biomedicine & Pharmacotherapy = Biomedecine & Pharmacotherapie. 2020; 129: 110239. https://doi.org/10.1016/j.biopha.2020.110239

[58] Deng G, Wang P, Su R, Sun X, Wu Z, Huang Z, et al. SPI1+CD68+ macrophages as a biomarker for gastric cancer metastasis: a rationale for combined antiangiogenic and immunotherapy strategies. Journal for Immunotherapy of Cancer. 2024; 12: e009983. https://doi.org/10.1136/jitc-2024-009983

[59] Gao Q, Wang Y. LncRNA FTX Regulates Angiogenesis Through miR-342-3p/SPI1 Axis in Stroke. Neuropsychiatric Disease and Treatment. 2021; 17: 3617–3625. https://doi.org/10.2147/NDT.S337774

[60] Starke RM, Chalouhi N, Ding D, Raper DMS, Mckisic MS, Owens GK, et al. Vascular smooth muscle cells in cerebral aneurysm pathogenesis. Translational Stroke Research. 2014; 5: 338–346. https://doi.org/10.1007/s12975-013-0290-1

[61] Shao Y, Zheng Q, Wang W, Xin N, Song X, Zhao C. Biological functions of macrophage-derived Wnt5a, and its roles in human diseases. Oncotarget. 2016; 7: 67674–67684. https://doi.org/10.18632/oncotarget.11874

[62] Wang K, Ma F, Arai S, Wang Y, Varkaris A, Poluben L, et al. WNT5a Signaling through ROR2 Activates the Hippo Pathway to Suppress YAP1 Activity and Tumor Growth. Cancer Research. 2023; 83: 1016–1030. https://doi.org/10.1158/0008-5472.CAN-22-3003

[63] van Amerongen R, Nusse R. Towards an integrated view of Wnt signaling in development. Development (Cambridge, England). 2009; 136: 3205–3214. https://doi.org/10.1242/dev.033910

[64] Mikels AJ, Nusse R. Purified Wnt5a protein activates or inhibits beta-catenin-TCF signaling depending on receptor context. PLoS Biology. 2006; 4: e115. https://doi.org/10.1371/journal.pbio.0040115

[65] Mehdawi LM, Ghatak S, Chakraborty P, Sjölander A, Andersson T. LGR5 Expression Predicting Poor Prognosis Is Negatively Correlated with WNT5A in Colon Cancer. Cells. 2023; 12: 2658. https://doi.org/10.3390/cells12222658

[66] Lyon C, Mill C, Tsaousi A, Williams H, George S. Regulation of VSMC behavior by the cadherin-catenin complex. Frontiers in Bioscience (Landmark Edition). 2011; 16: 644–657. https://doi.org/10.2741/3711

[67] Rong Z, Li F, Zhang R, Niu S, Di X, Ni L, et al. Ant-Neointimal Formation Effects of SLC6A6 in Preventing Vascular Smooth Muscle Cell Proliferation and Migration via Wnt/β-Catenin Signaling. International Journal of Molecular Sciences. 2023; 24: 3018. https://doi.org/10.3390/ijms24033018

[68] Di M, Wang J, Sun L, Yang G, Xu Q. E2F5 Accelerates Vascular Smooth Muscle Cells Phenotype Switching in Diabetic Atherosclerosis through Activating Wnt/β-Catenin Pathway. Diabetes & Metabolism Journal. 2026; 50: 506–518. https://doi.org/10.4093/dmj.2024.0588